

Deposit licences

Emerald allows authors to deposit their AAM under the Creative Commons Attribution Non-commercial International Licence 4.0 (CC BY-NC 4.0). To do this, the deposit must clearly state that the AAM is deposited under this licence and that any reuse is allowed in accordance with the terms outlined by the licence. To reuse the AAM for commercial purposes, permission should be sought by contacting permissions@emeraldinsight.com.



PAPER IS NOW PUBLISHED and can be accessed here: [DOI 10.1108/RPJ-12-2018-0316]
<https://www.emerald.com/insight/content/doi/10.1108/RPJ-12-2018-0316/full/html?skipTracking=true>

SUBMITTED VERSION

Impact of processing parameters on tensile strength, in-process crystallinity and mesostructure in FDM-fabricated PLA specimens

Journal:	<i>Rapid Prototyping Journal</i>
Manuscript ID	RPJ-12-2018-0316
Manuscript Type:	Original Article
Keywords:	Tensile strength, Crystallinity, Polylactic Acid, Build plate temperature, Definitive Screening Design, Mesostructure

SCHOLARONE™
Manuscripts

AUTHORS

Ognjan Luzanin and Dejan Movrin
 Department for Production Engineering, University of Novi Sad, Novi Sad, Serbia

Vassilis Stathopoulos and Pavlos Pandis
 Technological Educational Institute of Sterea Ellada, School of Technological Applications, Evia, Greece

Tanja Radusin
 Institute for Food Technology, Novi Sad, Serbia, and

Vera Guduric
 Centre for Translational Bone, Joint and Soft Tissue Research, Technische Universitat Dresden, Dresden, Germany

Deposit licences

Emerald allows authors to deposit their AAM under the Creative Commons Attribution Non-commercial International Licence 4.0 (CC BY-NC 4.0). To do this, the deposit must clearly state that the AAM is deposited under this licence and that any reuse is allowed in accordance with the terms outlined by the licence. To reuse the AAM for commercial purposes, permission should be sought by contacting permissions@emeraldinsight.com.

<https://www.emerald.com/insight/content/doi/10.1108/RPJ-12-2018-0316/full/html?skipTracking=true>

Impact of processing parameters on tensile strength, in-process crystallinity and mesostructure

Deposit licences in FDM-fabricated PLA specimens

Emerald allows authors to deposit their Creative Commons Attribution Non-commercial International Licence 4.0 (CC BY-NC 4.0). To do this, the deposit must clearly state that the AAM is deposited under this licence and that any reuse is allowed in accordance with the terms outlined by the licence. To reuse the AAM for commercial purposes, permission should be sought by contacting permissions@emeraldinsight.com.

Abstract

Purpose - This study investigates the impact of layer thickness, extrusion temperature, extrusion speed and build plate temperature on the tensile strength, crystallinity achieved during fabrication (herein, in-process crystallinity), and mesostructure of Poly(lactic acid) specimens. Both tensile strength and in-process crystallinity were optimized and verified as the function of processing parameters, and their relationship was thoroughly examined.

Design/Methodology/Approach - The four key technological parameters were systematically varied as factors on three levels, using the statistically designed experiment. Surface Response methodology was used to optimize tensile strength and crystallinity for the given ranges of input factors. Optimized factor settings were used in a set of confirmation runs, where the result of optimization was experimentally confirmed. Material characterization was performed using Differential Scanning Calorimetry (DSC), Fourier Transform Infrared spectroscopy (FTIR) and X-ray Diffraction analysis (XRD), while the effect of processing parameters on mesostructure was examined by SEM microscopy.

Findings - Layer thickness and its quadratic effect are dominant contributors to tensile strength. Significant interaction between layer thickness and extrusion speed implies that these parameters should always be varied simultaneously within designed experiment in order to obtain adequate process model. As regards the in-process crystallinity, extrusion speed is part of two significant interactions with plate temperature and layer thickness, respectively. Quality of mesostructure is vital contributor to tensile strength during FDM process, while the in-process crystallinity exhibited no impact, remaining below the 20% margin regardless of process parameter settings.

Originality - According to available literature, there have been no previously published investigations which studied the effect of process parameters on tensile strength, mesostructure, and in-process crystallinity through systematic variation of four critical processing parameters.

Key words: Fused Deposition Modelling (FDM), Definitive Screening Design (DSD), Tensile strength, Mesostructure, Crystallinity

1. Introduction

In principle a simple and arguably the most popular of all Additive Manufacturing technologies, Fused Deposition Modelling (FDM) is underpinned by a complex process with numerous parameters and their interactions that impact both product quality and final material properties. Given the substantial advances made in polymer engineering and the continuous improvement of FDM technology, fabrication of functional parts has become a viable option (Bourell, 2016). However, in order for FDM to become a mature and proven manufacturing tool, the mechanical properties of the parts should be further improved so as to allow them to maintain their integrity during service (Sun *et al.*, 2008). Unlike injection molding technology, which produces completely solid thermoplastic parts, FDM-built parts exhibit porous mesostructure. The formation of bonds in FDM process is driven by the thermal energy of semi-molten material (Li *et al.*, 2002). The voids which are present within the mesostructure, result from the incomplete diffusion occurring at the interfaces of adjacently laid-down polymer strands (Wang and Gardner, 2018), and represent an important concentration of stress which is responsible for possible material failure under stress. Therefore, mechanical properties are largely determined by the thermal history and the amount of diffused polymer chains (Faes, Ferraris and Moens, 2016; Bähr and Westkämper, 2018), which, in turn, depend on the selected processing parameters. Previous studies also indicate that, to a certain extent, FDM process promotes increase in crystallinity (Drummer, Cifuentes-Cuellar and Rietzel, 2012; Cuiffo *et al.*, 2017; Levenhagen and Dadmun, 2017; Song *et al.*, 2017), which impacts several important polymer properties, including hardness, modulus, tensile strength, stiffness, crease and melting points (Farah, Anderson and Langer, 2016). Desirable level of crystallinity depends on the application domain of FDM-fabricated parts. Thus, for example, it should be maximized to obtain mechanical properties and thermal stability of mechanical components, while in the case of scaffolds, crystallinity must be limited to provide adequate biodegradation kinetics, control toxicity, etc. From this point of view it is also interesting to observe the influence of the selection of FDM processing parameters on the crystallinity of fabricated parts.

With the previous discussion in mind, researchers have used various approaches to address the problem of FDM processing parameters and their influence on mechanical properties of parts, mesostructure, and crystallinity. Sun *et al.* (Sun *et al.*, 2008) investigated thermal profiles of some simple shapes of ABS, produced by the FDM, their effects on the bond formation in terms of neck growth between adjacent filaments and the intermolecular diffusion at the interface. Experimenting with three envelope and extrusion temperatures, they evaluated bond quality based on the growth of the neck formed between adjacent filaments, concluding that thermal history has important impact on the final mesostructure and bond strength. Sood *et al.* (Sood, Ohdar and Mahapatra, 2010) used central composite design (CCD) to analyse the impact of five process parameters: layer thickness, orientation, raster

1 angle, raster width and air gap on the three responses: tensile, flexural and impact strength of test specimens.
2
3 Regarding the thermal history of the part, they found that higher number of layers contributes to higher
4 temperature gradient towards the bottom of part, which, in turn, increases the diffusion between adjacent rasters,
5 contributing to strength improvement. Similarly, higher infill and wider raster allowed improved diffusion and
6 stronger bond formation. Drummer et al. (Drummer, Cifuentes-Cuéllar and Rietzel, 2012) investigated the
7 problem of general suitability of PLA and TCP for FDM processing. They focused on understanding the thermal
8 effects that occur in PLA as the consequence of FDM extrusion. PLA crystallization and shrinkage were examined
9 as the function of FDM processing parameters, followed by thermal, mechanical, and microscopic analyses. Based
10 on the results, they found a remarkable relation between processing temperature and morphology, where a higher
11 degree of crystallinity corresponded to higher extrusion temperature. Wittbrodt and Pearce (Wittbrodt and Pearce,
12 2015) examined the case of five filament colors of commercially available filament processed from 4043D PLA,
13 and tested them for crystallinity with XRD. In the part which pertains to our discussion, their results showed
14 strong relationship between tensile strength and percent crystallinity of a 3-D printed sample and a strong
15 relationship between percent crystallinity and the extruder temperature. Davis et al. (Davis et al., 2017) focused
16 on the impact of process parameters on the strength of the weld zones using a consumer-grade FDM printer and
17 commercial ABS material. They varied extrusion temperature (210-250 °C) and extruder velocity (1-100 mm/s),
18 keeping layer thickness constant at 0.3 mm. They found that extrusion temperature and velocity impacted weld
19 strength, i.e., maximum strength was yielded by highest extrusion temperature and velocity. Chacón
20 et al. (Chacón et al., 2017) investigated the effect of build orientation, layer thickness and feed rate on the mechanical
21 performance of PLA samples manufactured with a low cost 3D printer. They varied build orientation, layer
22 thickness, and extrusion speed with the adjusted flow rate, examining tensile and flexural strength of the samples
23 fabricated on a consumer class 3D printer. The effect of layer thickness was a function of build orientation.
24 Specifically, for the flat oriented specimens, layer thickness of 0.06 mm yielded higher tensile and lower flexural
25 strength. In their study, the effect of extrusion speed was not significant for the flat oriented specimens, regarding
26 both the tensile and flexural strength. Wang et al. (Wang, Gramlich and Gardner, 2017) investigated the impact
27 of two printing parameters - layer height (0.2 and 0.4 mm) and plate temperature (30 and 160 °C) - on the Izod
28 impact strength of printed PLA. X-ray diffraction (XRD) analysis confirmed the existence of crystals in parts
29 printed from 160 °C-plate temperature and α_0 crystals in those printed at 30 °C-plate temperature. Parts printed
30 with a 160 °C (plate temperature) had higher crystallinity. Polarized optical microscope (POM) observations
31 illustrated that the plate temperature of 160 °C and layer height of 0.2 mm induced higher crystallinity, smaller
32 crystals and interfacial crystal bands. Aliheidari et al. (Aliheidari et al., 2018) investigated the relationships
33
34
35
36
37
38
39
40
41
42
43
44
45
46
47
48
49
50
51
52
53
54
55
56
57
58
59
60

1
2 between the process parameters, mesostructural features (interlayer neck and void sizes), and the fracture
3 resistance of 3D printed parts. The aim was to investigate the influence of bond quality and mesostructure on the
4 overall fracture behaviour of the acrylonitrile butadiene styrene (ABS) specimens. Selecting nozzle temperature,
5 plate temperature, layer height, and layer width as study parameters, they found that nozzle and bed temperatures
6 and layer height had significant effects on the fracture behaviour. Song et al. (Song *et al.*, 2017) studied the
7 problem of orthotropic mechanical response of 3D-printed PLA. PLA blocks were fabricated by FDM technology,
8 using unidirectional deposition. Specimens were cut from printed blocks using conventional machining for the
9 purpose of tension, compression and fracture testing along different material directions. They concluded that the
10 mechanical response of the specimens can be improved by optimising the extrusion temperature and extrusion
11 speed. In addition, they found that manufacturing by 3D-printing increases the crystallinity of the material.

12
13
14
15
16
17
18
19
20
21 Previous investigations show that part quality and final material properties are sensitive to processing parameters,
22 as they significantly affect the meso-structure and bond strength between deposited roads. Both the experiments
23 and numerical simulations imply that the variations in layer thickness and extrusion speed, respectively, impact
24 the change in mean temperature of the deposited layers (Zhang *et al.*, 2017). In addition, variable heating and
25 cooling cycles result in accumulation of internal stresses, which in turn cause weak bonding and mesostructural
26 voids, affecting the final strength (Sood, Ohdar and Mahapatra, 2010). Thus, beside layer thickness and extrusion
27 speed, there are extrusion temperature, temperature of build plate and the envelope, which also have crucial
28 influence on temperature variation during extrusion. However, the review of literature sources showed lack of
29 investigations which used statistically designed experiment to systematically vary the four crucial processing
30 parameters: layer thickness, extrusion speed, extrusion temperature, and build plate temperature to investigate
31 their aggregate impact on mechanical and other properties of FDM-fabricated parts. With this in mind, the present
32 study investigates the impact of these four key processing parameters on the tensile strength, in-process
33 crystallinity, and mesostructure of PLA specimens. Considering the fact that a consumer class 3D printer will be
34 used, only the envelope temperature will not be taken into consideration as a controllable factor. A statistically
35 designed experiment shall be used to investigate the influence of main factors and their interactions, while the
36 processing parameters shall be optimized for maximum tensile strength and verified through additional
37 confirmation runs. Furthermore, the same experiment shall be used to investigate change in material crystallinity,
38 allowing us to shed additional light on the combined impact of plate temperature, layer thickness, extrusion speed,
39 extrusion temperature, and their interactions, on this important material property.

2. Experimental design, materials and methods

2.1 Design of experiment and processing parameters

The design of this experiment is based on the Definitive Screening Design (DSD) (Jones and Nachtsheim, 2011; Xiao, Lin and Bai, 2012) and the response surface methodology (RSM). The DSD method has recently gained popularity because, it allows reduction of the total number of experiments required to estimate main effects, quadratic effects, and some two-factor interactions, most often without the follow-up experimentation to resolve confoundings. The DSD has seen recent FDM-related applications in (Luzanin *et al.*, 2017; Mohamed, Masood and Bhowmik, 2017). Table 1 shows the four processing parameters with their low, center, and high settings.

It should be noted that although our printer's build plate is capable of reaching 120 °C, preliminary experiments showed that some extreme parameter combinations lead to thermal runaway error, requiring us to limit the build plate temperature in this experiment to 80 °C. Another reason for this limitation was the preservation of PLA specimen integrity, since higher plate temperatures resulted in very soft specimen bottom, which could easily lead to deformation during removal from the build plate, and affect the subsequent tensile strength testing. The remaining important processing parameters which were kept constant during experiment, are listed in Table 2.

Considering the number of DSD runs, four continuous factors ($k=4$) would theoretically require $2k+1$ runs, i.e., 9 experiments. However, as recently shown in (Jones and Nachtsheim, 2017) the addition of two fake factors ($k=6$) allows estimation of pure error under the assumption that third-order interactions are negligible, which is most often the case. Furthermore, with the addition of four extra runs and two replications at the centre point, the total number of runs adds up to $2k+1+4+2=19$ runs. These extra runs are meant to enable the design of experiment to have more statistical power, as well as to reliably identify higher number of second-order effects without confounding. The resulting table of experiment with 19 runs is shown in Tab. 3.

2.2 Specimen fabrication

Prusa i3 MK2S consumer-class FDM printer with a steel 0.4 mm nozzle and a freshly unpacked 1.75 mm yellow PLA filament from *3D-Fuel* (USA) were used to fabricate all specimens used in the experiment. The 19 specimens were fabricated according to the settings given in Table 3, in a randomized order, and within a single session, without intermissions. Each specimen was fabricated so that its dominant dimension was oriented parallel to printer's X-axis, using alternate (0/90°) raster orientation (Fig. 1). In order to assess stability of the process, the three specimens which correspond to centre point, were printed at the beginning, the middle, and the end of the experimental session.

2.3 Tensile tests

Universal tester, *Shimadzu EZ-LX*, was used to test the specimens for tensile strength in compliance with the ISO 527-2: 2012 specification (ISO 527-2, 2012). Crosshead speed of 50 mm/min was used, while the tests were conducted at 24 °C. Tensile force and the resulting stress are shown in Table 3.

2.4 Differential Scanning Calorimetry (DSC) analysis of crystallinity

DSC analysis was performed with *Setaram STA* (France) unit, under pure (99,99%) nitrogen with a total flow of 20 ml/min. DSC curves were recorded in the range of 25 to 220 °C for all the samples with a heating rate of 10 °C/min. Computational integration of thermal phenomena peaks for the enthalpy and crystallinity was done using *Calisto Processing 2.1* software. Percent crystallinity was calculated based on equation (1) (Ahmed *et al.*, 2009):

$$X_c = \frac{\Delta H_m - \Delta H_{cc} - \Delta H_r}{\Delta H_f} \quad (1)$$

where ΔH_m , ΔH_{cc} , and ΔH_r are the enthalpies of melting, cold crystallization and reordering of polymer chains, respectively. The heat of fusion (ΔH_f), which corresponds to 100% melting enthalpy of crystalline PLA, was adopted as 93 J/g (Ahmed *et al.*, 2009). The results are presented in Fig. 6, and in Tab. 4, with the resulting crystallinity percent given in the rightmost column.

2.5 Fourier Transformed Infrared Spectroscopy Analysis (FTIR)

FTIR analysis was performed on *ALPHA Bruker* (Germany). The spectra were taken in the interval between 4000 and 400 cm^{-1} wavelengths with 4 cm^{-1} resolution. To ensure reliability of data, each analysed spectrum was calculated as a mean of 24 recordings. The diagrams for the discussion of FTIR analysis are given in Fig. 7, for the three representative samples.

2.6 X-Ray Diffraction Analysis (XRD)

XRD patterns were obtained on *Rigaku MiniFlex 600* diffractometer (operating at 40 kV and 15 mA, using Cu $K\alpha$ radiation). Patterns were obtained in continuous mode, at a 3 deg/min rate. For the selected samples, both top and bottom surfaces were examined, as shown in Fig. 11.

2.7 Scanning Electron Microscopy (SEM)

Mesostructure was examined on specimen cross-sections using a scanning electron microscope, *SEM JEOL JSM 6460 LV*. To provide mesostructure undistorted by tensile tests, the samples were soaked in liquid nitrogen and cryofractured. All images were taken at an accelerating voltage of 20 kV at 40x and 100x magnification in backscatter mode (BEI). Thus obtained, SEM micrographs were further analysed in Fiji software (Schindelin *et al.*, 2012).

3. Results and analysis

Statistical analyses were performed in SAS JMP r13, while the results for both tensile strength and crystallinity are presented through optimization plots (Fig. 2, 3), parameter estimates (Tab. 5 and 8), summary of fit (Tab. 6 and 9), ANOVA table (Tab. 7 and 10) and surface/contour plots (Fig. 4 a-f).

3.1 Statistical analysis of results for tensile strength

For tensile strength, layer thickness and its quadratic term exhibit statistical significance which also reflects in the magnitude of their estimates (Tab. 5). A look at the optimization profiler (Fig. 2) reveals that optimum tensile strength is obtained when layer thickness is at its mid-level, i.e., 0.2 mm. Due to significance of the quadratic effect, moving in both directions away from this optimal point, has a pronounced effect on the tensile strength, causing its reduction.

A statistically significant interaction between layer thickness (LT) and extrusion speed (ES) can be observed from surface plots shown in Fig. 4. When layer thickness is kept constant, at 0.1 mm, tensile strength increases as the extrusion speed decreases (Fig. 4 a,b). The same holds true for layer thickness 0.2 mm, where the optimum is reached at 30 mm/s extrusion speed. However, this trend reverses when layer thickness is kept constant at 0.3 mm (Fig. 4 a,b), where it is obvious that tensile strength slightly increases as the extrusion speed picks up.

3.2 Statistical analysis of results for crystallinity

In the case of crystallinity, the fitted model is more complex. Table 8 lists all terms in the ascending order of their p-value. The effect of quadratic terms can be most easily observed in the profiler (Fig. 3), while the two-way interactions are best discussed using surface and contour plots (Fig. 4 c-f).

As seen from Table 8, extrusion speed is involved in two significant interactions. The interaction between extrusion speed (ES) and layer thickness (LT) is shown in Fig. 4 c,d. When extrusion speed is kept constant at low level (ES=30 mm/s), crystallinity increases as the layer thickness goes from low level (LT=0.1 mm), towards high level (LT=0.3 mm). Although less prominent, the same trend is observed when extrusion speed is kept constant at its mid-level (Fig. 4 c,d). However, at high level of extrusion speed (ES=90 mm/s), the opposite trend is observed, where crystallinity drops as the layer thickness increases from 0.1 to 0.3 mm (Fig. 4 c,d).

The remaining significant interaction which involves extrusion speed (ES) and plate temperature (PT) is shown in Fig. 4 e,f. As seen from the surface plot (Fig. 4e), the interaction is represented by a hyperbolic paraboloid. In this regard, contour plot is more useful. As seen in Fig. 4f, the depression runs through the middle of the diagram, which corresponds to a strip around the mid-level of plate temperature (PT=65 °C). When the extrusion speed is kept at its low level, crystallinity varies as plate temperature increases, reaching minimum in the region 55-65 °C and climbing to its maximum as the plate temperature reaches high level (Fig. 4f). Conversely, when the extrusion

1 speed is constant at ES=90 mm/s, heating the build plate from 50 to 80 °C leads to a constant drop in crystallinity,
2 which turns just slightly upward when the plate reaches maximum temperature (better seen on the right-hand side
3 of the surface plot, Fig. 4e). Finally, the quadratic term involving extrusion temperature (ET) (Tab. 8) is also
4 statistically significant. As seen from the optimization plot (Fig. 3), the optimal ET is found at 220 °C. Due to the
5 quadratic effect, moving in either direction from that optimal point results in the drop of percent crystallinity.
6
7
8
9

10 3.3 Verification of the predicted optimal response for tensile strength and crystallinity

11 Tensile strength optimized by the adopted regression model based on the design of experiment, was
12 experimentally verified by testing an additional battery of specimens fabricated with the optimized process
13 parameters. Based on the results thus obtained, a 95% confidence interval was calculated, to check whether it
14 contains the numerically optimized tensile strength (Willis, 2016). The additional ten specimens were fabricated
15 within a single session, on the same 3D printer, using the optimized settings shown in the profiler plot (Fig. 2).
16 The results of tensile stress testing are listed in Tab. 11, while the resulting 95% confidence interval was calculated
17 as CI [61.98, 65.96]. The tensile strength value of 65.77 MPa, optimized by the adopted regression model (Fig.
18 2), falls within the confirmatory run confidence interval (Fig. 5), meaning that the model successfully passed the
19 confirmation test.
20
21
22
23
24
25
26
27
28
29

30 Considering the fact that by measuring crystallinity one is indirectly examining the increase in local order within
31 the polymer matrix, the presence of higher standard deviation is understandable. Rather than giving them absolute
32 meaning, the results obtained should be treated as a helpful means to establish necessary correlations to understand
33 other material properties, or in our case, the effect of process parameters. With this caution in mind, similar to the
34 tensile strength, the experimental verification was performed to determine whether the adopted regression model
35 yields results within a required margin and whether it can be used to discuss the influence of process parameters
36 on crystallinity. The results of five additional crystallinity measurements obtained for the samples printed with
37 parameters optimized for maximum crystallinity (Fig. 3) are shown in Table 12. The calculated 95% confidence
38 interval for the mean crystallinity $M=16.48$, CI [13.3, 19.6] contains the value of 19.44, predicted by the adopted
39 regression model, which, bearing in mind previous notes, allows this model to be used for further discussion.
40
41
42
43
44
45
46
47
48
49

50 3.4 DSC thermograms

51 Figure 6 shows a comparative plot of the DSC thermograms of as-received PLA filament, specimen #1, and
52 specimen #13 as the specimens which exhibited the lowest and highest crystallinity, respectively. The diagram
53 shows three features which are characteristic for semi-crystalline thermoplastics, glass transition, cold
54 crystallization, and melting (Fig. 6). Regarding neat PLA, its glass transition temperature (T_g) is close to 60 °C
55 and is clearly detectable by a change in slope. The exothermic peak comprised between 90 and 110 °C is related
56
57
58
59
60

1
2 to the cold crystallization process while the endothermic peak between 150 and 180 °C corresponds to the melting
3 process. The clearly visible, small exothermic peak that precedes the melting peak on each diagram is attributed
4 to the re-ordering of PLA. Namely, at temperatures close to the melting temperature (in our experiment, 170 °C),
5 the spherulites (α' form) of the PLA generated at temperatures close to 100 °C, are disordered. The exothermic
6 peaks visible in Fig. 6 are related to the α' to α phase transition, followed by the melting of the newly developed
7 α phase (Tábi, Hajba and Kovács, 2016; Ferri *et al.*, 2018).
8
9

10 11 12 13 14 3.5 FTIR diagrams

15 FTIR analysis reveals the presence of absorption maxima at characteristic wavelength bands marked in color (Fig.
16 7). Absorption maxima at wavelengths around 2900, belonging to band I, correspond to C-H stretching vibrations
17 of aliphatic carbohydrates, while the peaks belonging to band II (1754, 1745, and 1749 cm^{-1}) indicate the presence
18 of C=O molecular group. Absorption maxima at wavelengths 1490, 1455 and 1359 cm^{-1} (band III), come from
19 deforming CH_3 and CH_2 symmetrical and asymmetrical vibrations, respectively. C-O-C asymmetric stretching is
20 present at 1078 cm^{-1} (band IV). Peaks at 2305 and 2360 cm^{-1} which can be observed in the case of PLA filament
21 and specimen 16, respectively (Fig. 7 a and c), are attributed to CO_2 contamination and are not related to particular
22 aspects of the FDM process, i.e., processing parameters.
23
24
25
26
27
28
29
30

31 32 4. Discussion

33 According to results of the tensile strength analysis, the layer height of 0.2 mm yields maximum tensile strength,
34 which was also reported in previous experimental studies with PLA (Tymrak, Kreiger and Pearce, 2014; Lanzotti
35 *et al.*, 2015) and ABS (Aliheidari *et al.*, 2018). This finding can be explained by the cross-sectional geometry of
36 deposited roads, which obviously depends on the ratio between nozzle diameter and layer thickness. In the case
37 of a 0.4 mm nozzle, which is standard in most consumer-grade FDM printers, the cross-section varies as the layer
38 thickness (LT) changes from 0.1 to 0.3 mm, as shown in Fig. 8. In the case of layer height 0.1 and 0.2 mm (Fig.
39 8a,b), due to nozzle diameter/layer height ratio, higher contact pressure stimulates molecular contact at the
40 interface, thus promoting the healing process. However, due to lower polymer mass extruded, there is a dominant
41 influence of the cooling rate on bond formation, which is why extrusion speed is negatively correlated with tensile
42 strength (Fig. 4 a,b). Alternatively, when printing with layer thickness of 0.3 mm, less contact pressure is exerted
43 from the extruder nozzle during road deposition, while the cross-sectional geometry is closer to circular (Fig. 8c),
44 resulting in diminished interlayer contact area. Our finding is also supported by Comminal *et al.* (Comminal *et*
45 *al.*, 2018), who discussed morphology of printed strands based on a CFD simulation. Also, Coogan *et al.* (Coogan
46 and Kazmer, 2017), discussed the importance of pressure for the intimate contact between thermoplastics, which
47 is required to overcome high melt viscosities. This means that the pressure from the extrusion head also contributes
48
49
50
51
52
53
54
55
56
57
58
59
60

1
2 to bond formation and its strength, as do the wetting and molecular diffusion. On the other hand, in the case of
3 high layer thickness (LT=0.3 mm), higher polymer mass extruded in combination with higher extrusion speed,
4 result in shorter processing time and higher mean temperature of specimen, which is beneficial for inter-layer
5 bonding, as previously shown in (Zhang *et al.*, 2017).
6
7

8
9 An effective illustration of the impact of layer thickness can be given from the mesostructural perspective (Fig.
10 9). Surface plot in Fig. 9a pertains to optimal tensile strength settings, yielded by the profiler (Fig. 2), where the
11 layer thickness of 0.2 mm is marked by the vertical grid. However, when the layer thickness shifts to 0.3 mm (Fig.
12 9c), all other settings remaining at their optimized values, this not only causes reduction in tensile strength, but is
13 also accompanied by visible changes in mesostructure (Fig. 9b,d). The most prominent detail of mesostructural
14 deterioration is the presence of larger air gaps (Fig. 9d), due to reduced quality of the healing process.
15
16

17
18 In the case of crystallinity, our finding that the plate temperature and its quadratic effect are dominant is in
19 concordance with the previous conclusion by Wang *et al.* (Wang, Gramlich and Gardner, 2017), who reported
20 that higher plate temperature generated higher crystallinity in PLA specimens. However, our results showed no
21 evident correlation between the increase of tensile strength and percent crystallinity obtained during the very FDM
22 process. This is graphically depicted in Fig. 10, where the dual Y axis diagram shows variations in crystallinity
23 while the specimen numbers are sorted by tensile strength in the ascending order. Experimenting with changes in
24 PLA crystallinity in a different study, Levenhagen *et al.* (Levenhagen and Dadmun, 2017) came to a similar
25 conclusion that there is no recognizable correlation between the mechanical properties and the extent of
26 crystallinity obtained solely during the FDM extrusion process.
27
28

29
30 To explain this phenomenon, one should consider the range of percent crystallinity obtained in this designed
31 experiment, including the optimized value. Namely, the as-received filament exhibited average crystallinity of
32 10%, while the maximum and minimum crystallinity values obtained by designed experiment and optimization,
33 were 5.3 and 19.6, respectively. Despite the ability of processing to change material crystallinity within the 15%
34 range, this in-process crystallinity remains low, which is why quality of mesostructure played the primary role in
35 achieving tensile strength.
36
37

38
39 As seen from the significant interaction (Fig. 4 c,d) when extrusion speed (ES) is kept constant at its high level,
40 crystallinity slumps with the increase of layer thickness (LT). The observed phenomenon is in conformance with
41 the discussion in (Wang, Gramlich and Gardner, 2017). Namely, the change in layer thickness requires adequate
42 change in the filament feeding rate, meaning that higher layer thickness exacts more material fed into extrusion
43 chamber per time unit. Higher material volume, in turn, results in cooler polymer melt, which, combined with the
44 faster movement of the hot extrusion head, means more rapid cooling of the deposited road. The characteristic
45
46
47
48
49
50
51
52
53
54
55
56
57
58
59
60

1 drop in crystallinity at medium plate temperature, observed in the interaction plots for plate temperature (PT) and
2 extrusion speed (ES) (Fig. 4 e,f) is also interesting, however, its explanation requires additional investigation.

3
4
5 Another phenomenon worth discussing is the mid-level extrusion temperature (ET) which in our experiment
6 corresponds to highest percent crystallinity (Fig. 3). Some previous studies (Drummer, Cifuentes-Cuéllar and
7 Rietzel, 2012; Wittbrodt and Pearce, 2015) suggested that higher extrusion temperature leads to higher percent
8 crystallinity. However, when approaching this subject, one should take into account that those studies did not
9 report extrusion speed (ES) as one of the controllable factors, which precludes direct comparison to our study.
10 Although this temperature setting was confirmed by the experimental verification (discussed in section 3.3), it
11 was additionally examined by XRD analysis. Shown in Fig. 11 are XRD profiles of the three specimens: #1, #2
12 and #17. As seen from Tab. 3, they were all printed with the same plate temperature (PT=65 °C), while their
13 extrusion temperatures (ET) were 230 °C, 210 °C and 220 °C, respectively. Considering the bottom specimen side,
14 which was in contact with the heated build plate (Fig. 11a), only specimen #17, printed with ET=220 °C, exhibits
15 a peak at $2\theta \approx 16.4^\circ$, which indicates the presence of crystalline regions, while the rest of the samples feature broad
16 halos indicative of predominantly amorphous structure. The upper-side XRD profiles feature no significant
17 difference between the samples (Fig. 11b). The phenomenon of stratified crystallinity in FDM-printed PLA
18 samples has already been reported by Drummer et al. (Drummer, Cifuentes-Cuéllar and Rietzel, 2012).

32 5. Conclusions

33
34
35 The purpose of this study was to investigate the impact of four key FDM processing parameters on the tensile
36 strength, mesostructure, and crystallinity of PLA specimens, fabricated on a consumer class 3D printer. The
37 processing parameters were optimized in a controlled statistical experiment for maximum tensile strength and
38 then verified through ten additional confirmation runs. Moreover, in order to investigate the possibility to control
39 percent crystallinity during the very fabrication process, the same processing parameters and their levels were
40 varied to investigate their contribution to crystallinity of material.

41 Systematic variation of the four selected process parameters revealed following:

- 42 • Layer thickness and its quadratic effect are dominant contributors to tensile strength. Layer thickness of
43 0.2 mm produced most compact mesostructure, yielding optimal values of tensile strength. The
44 contribution of layer thickness to the quality of mesostructure is the function of nozzle diameter.
- 45 • Extrusion speed plays an important role, being involved in a significant interaction with layer thickness
46 in both the tensile strength and crystallinity models. In the case of crystallinity, it also interacts with the
47 build plate temperature. This implies that extrusion speed should not be kept constant in experiments

1
2 dealing with FDM processing parameters, as has often been the case, since it allows us to obtain process
3 models which are closer to reality.

- 4 • The increase of in-process crystallinity is not correlated with the increase in tensile strength. This is due
5 to the fact that, even at its optimized level, the in-process crystallinity remains in the low region, i.e.,
6 below 20 %. However, this study showed that in-process crystallinity of the samples can be successfully
7 controlled by the proper selection of processing parameters levels, and varied within the 15% range. This
8 ability to reliably control the in-process crystallinity is important, and can prove very useful in biomedical
9 applications of FDM, where crystallinity highly affects a number of crucial biocompatibility features,
10 such as biodegradation kinetics, toxicity, etc.

11
12 With regard to future work, the importance of convection within the envelope during the FDM process is obvious
13 from previous simulations, which means that further experimental investigation should also include envelope
14 temperature and be investigated in more detail. The dimensional factor is also important, requiring extension of
15 this experiment on part geometries other than the standard specimens.

26 27 28 29 30 31 32 33 34 35 36 37 38 39 40 41 42 43 44 45 46 47 48 49 50 51 52 53 54 55 56 57 58 59 60

References

- Ahmed, J. *et al.* (2009) 'Thermal properties of polylactides: Effect of molecular mass and nature of lactide isomer', *Journal of Thermal Analysis and Calorimetry*, 95(3), pp. 957–964. doi: 10.1007/s10973-008-9035-x.
- Aliheidari, N. *et al.* (2018) 'Interlayer adhesion and fracture resistance of polymers printed through melt extrusion additive manufacturing process', *Materials & Design*, 156, pp. 351–361. doi: 10.1016/j.matdes.2018.07.001.
- Bähr, F. and Westkämper, E. (2018) 'Correlations between Influencing Parameters and Quality Properties of Components Produced by Fused Deposition Modeling', *Procedia CIRP* 72. pp.1214–1219. doi: 10.1016/j.procir.2018.03.048.
- Bourell, D. L. (2016) 'Perspectives on Additive Manufacturing', *Annual Review of Materials Research*, 46(1), pp. 1–18. doi: 10.1146/annurev-matsci-070115-031606.
- Chacón, J. M. *et al.* (2017) 'Additive manufacturing of PLA structures using fused deposition modelling: Effect of process parameters on mechanical properties and their optimal selection', *Materials and Design*, 124, pp. 143–157. doi: 10.1016/j.matdes.2017.03.065.
- Comminal, R. *et al.* (2018) 'Numerical modeling of the strand deposition flow in extrusion-based additive manufacturing', *Additive Manufacturing*, 20, pp. 68–76. doi: 10.1016/j.addma.2017.12.013.
- Coogan, T. J. and Kazmer, D. O. (2017) 'Healing simulation for bond strength prediction of FDM', *Rapid Prototyping Journal*, 23(3), pp. 551–561. doi: 10.1108/RPJ-03-2016-0051.
- Cuiffo, M. A. *et al.* (2017) 'Impact of the Fused Deposition (FDM) Printing Process on Polylactic Acid (PLA) Chemistry and Structure', *Applied Sciences*, 7(6), p. 579. doi: 10.3390/app7060579.

- 1
2 Davis, C. S. *et al.* (2017) 'Mechanical strength of welding zones produced by polymer extrusion additive
3 manufacturing', *Additive Manufacturing*, 16, pp. 162–166. doi: 10.1016/j.addma.2017.06.006.
4
- 5 Drummer, D., Cifuentes-Cuéllar, S. and Rietzel, D. (2012) 'Suitability of PLA/TCP for fused deposition
6 modeling', *Rapid Prototyping Journal*, 18(6), pp. 500–507. doi: 10.1108/13552541211272045.
7
- 8
9 Faes, M., Ferraris, E. and Moens, D. (2016) 'Influence of Inter-layer Cooling time on the Quasi-static Properties
10 of ABS Components Produced via Fused Deposition Modelling', *Procedia CIRP* 42, pp. 748–753. doi:
11 10.1016/j.procir.2016.02.313.
12
- 13
14 Farah, S., Anderson, D. G. and Langer, R. (2016) 'Physical and mechanical properties of PLA, and their
15 functions in widespread applications — A comprehensive review', *Advanced Drug Delivery Reviews*, 107, pp.
16 367–392. doi: 10.1016/j.addr.2016.06.012.
17
- 18
19 Ferri, J. M. *et al.* (2018) 'Poly(lactic acid) formulations with improved toughness by physical blending with
20 thermoplastic starch', *Journal of Applied Polymer Science*, 135(4), pp. 1–8. doi: 10.1002/app.45751.
21
- 22 'ISO 527-2: 2012. Plastics -- Determination of tensile properties -- Part 2: Test conditions for moulding and
23 extrusion plastics.pdf' (no date).
24
- 25
26 Jones, B. and Nachtsheim, C. J. (2011) 'A Class of Three-Level Designs for Definitive Screening in the
27 Presence of Second-Order Effects', *Journal of Quality Technology*, 43(1), pp. 1–15.
28
- 29
30 Jones, B. and Nachtsheim, C. J. (2017) 'Effective Design-Based Model Selection for Definitive Screening
31 Designs', *Technometrics*, 59(3), pp. 319–329. doi: 10.1080/00401706.2016.1234979.
32
- 33
34 Lanzotti, A. *et al.* (2015) 'The impact of process parameters on mechanical properties of parts fabricated in PLA
35 with an open-source 3-D printer', *Rapid Prototyping Journal*, 21(5), pp. 604–617. doi: 10.1108/RPJ-09-2014-
36 0135.
37
- 38
39 Levenhagen, N. P. and Dadmun, M. D. (2017) 'Bimodal molecular weight samples improve the isotropy of 3D
40 printed polymeric samples', *Polymer (United Kingdom)*, 122, pp. 232–241.
41 doi: 10.1016/j.polymer.2017.06.057.
42
- 43
44 Li, L. *et al.* (2002) 'Investigation of bond formation in FDM process', *Solid Freeform Fabrication Proceedings*,
45 (403), pp. 400–407. doi: 10.1108/13552540810862028.
46
- 47
48 Luzanin, O. *et al.* (2017) 'Investigating impact of five build parameters on the maximum flexural force in FDM
49 specimens - A definitive screening design approach', *Rapid Prototyping Journal*, 23(6). doi: 10.1108/RPJ-09-
50 2015-0116.
51
- 52
53 Mohamed, O. A., Masood, S. H. and Bhowmik, J. L. (2017) 'Influence of processing parameters on creep and
54 recovery behavior of FDM manufactured part using definitive screening design and ANN', *Rapid Prototyping
55 Journal*, 23(6), pp. 998–1010. doi: 10.1108/RPJ-12-2015-0198.
56
- 57
58 Schindelin, J. *et al.* (2012) 'Fiji: An open-source platform for biological-image analysis', *Nature Methods*, 9(7),
59 pp. 676–682. doi: 10.1038/nmeth.2019.
60

- 1
2 Song, Y. *et al.* (2017) 'Measurements of the mechanical response of unidirectional 3D-printed PLA', *Materials*
3 *and Design*, 123, pp. 154–164. doi: 10.1016/j.matdes.2017.03.051.
4
- 5 Sood, A. K., Ohdar, R. K. and Mahapatra, S. S. (2010) 'Parametric appraisal of mechanical property of fused
6 deposition modelling processed parts', *Materials & Design*. Elsevier Ltd, 31(1), pp. 287–295. doi:
7 10.1016/j.matdes.2009.06.016.
8
9
- 10 Sun, Q. *et al.* (2008) 'Effect of processing conditions on the bonding quality of FDM polymer filaments', *Rapid*
11 *Prototyping Journal*, 14(2), pp. 72–80. doi: 10.1108/13552540810862028.
12
13
- 14 Tábi, T., Hajba, S. and Kovács, J. G. (2016) 'Effect of crystalline forms (α' and α) of poly(lactic acid) on its
15 mechanical, thermo-mechanical, heat deflection temperature and creep properties', *European Polymer*
16 *Journal*, 82, pp. 232–243. doi: 10.1016/j.eurpolymj.2016.07.024.
17
18
- 19 Tymrak, B. M., Kreiger, M. and Pearce, J. M. (2014) 'Mechanical properties of components fabricated with
20 open-source 3-D printers under realistic environmental conditions', *Materials and Design*, 58, pp. 242–246.
21 doi: 10.1016/j.matdes.2014.02.038.
22
23
- 24 Wang, L. and Gardner, D. J. (2018) 'Contribution of printing parameters to the interfacial strength of polylactic
25 acid (PLA) in material extrusion additive manufacturing', *Progress in Additive Manufacturing*. Springer
26 International Publishing, 3(3), pp.165-171, doi: 10.1007/s40964-018-0041-7.
27
28
- 29 Wang, L., Gramlich, W. M. and Gardner, D. J. (2017) 'Improving the impact strength of Poly(lactic acid) (PLA)
30 in fused layer modeling (FLM)', *Polymer (United Kingdom)*, 114, pp. 242–248.
31 doi: 10.1016/j.polymer.2017.03.011.
32
33
- 34 Willis, A. (2016) 'Confirmation Runs in Design of Experiments', *Journal of Quality Technology*, 48(2),
35 pp. 162–177.
36
37
- 38 Wittbrodt, B. and Pearce, J. M. (2015) 'The effects of PLA color on material properties of 3-D printed
39 components', *Additive Manufacturing*, 8, pp. 110–116. doi: 10.1016/j.addma.2015.09.006.
40
41
- 42 Xiao, L., Lin, D. K. J. and Bai, F. (2012) 'Constructing definitive screening designs using conference matrices',
43 *Journal of Quality Technology*, 44(1), pp. 2–8. doi: 10.1080/00224065.2012.11917877.
44
45
- 46 Zhang, J. *et al.* (2017) 'Numerical investigation of the influence of process conditions on the temperature
47 variation in fused deposition modeling', *Materials and Design*, 130, pp. 59–68. doi:
48 10.1016/j.matdes.2017.05.040.
49
50
51
52
53
54
55
56
57
58
59
60

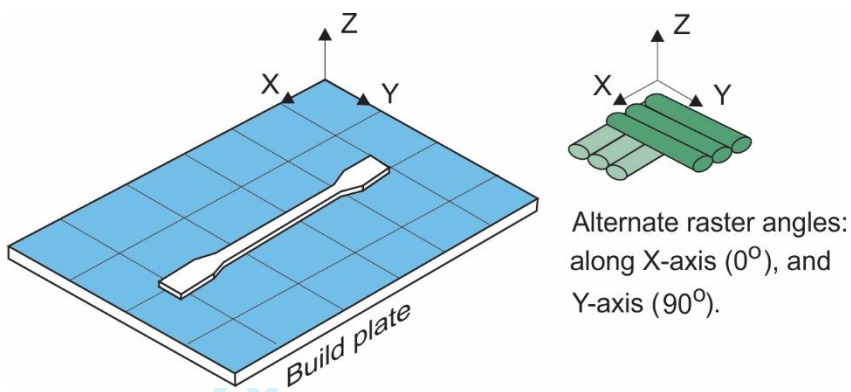


Fig. 1. Specimen orientation and raster orientation used in the designed experiment.

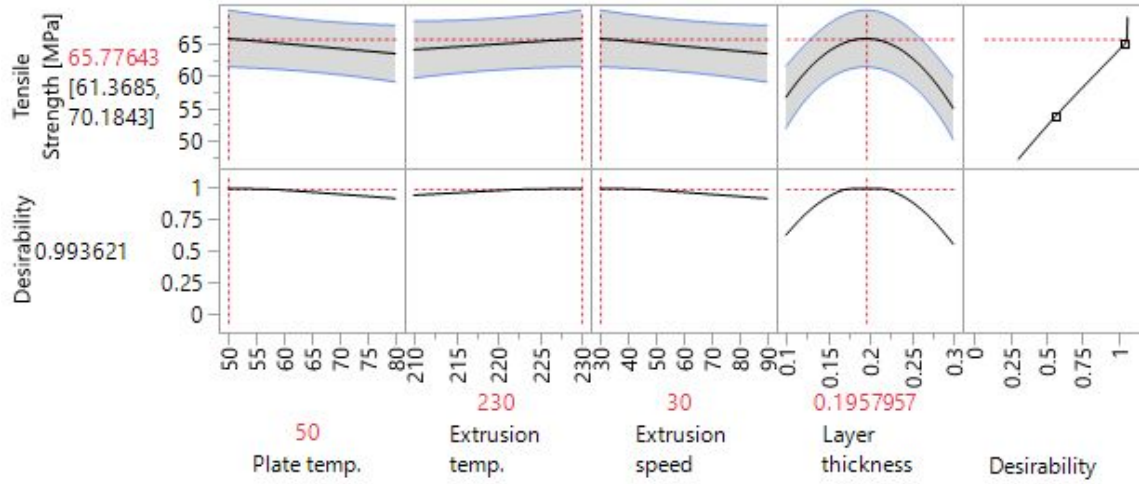


Fig. 2. Optimization plot for the Tensile strength experiment.

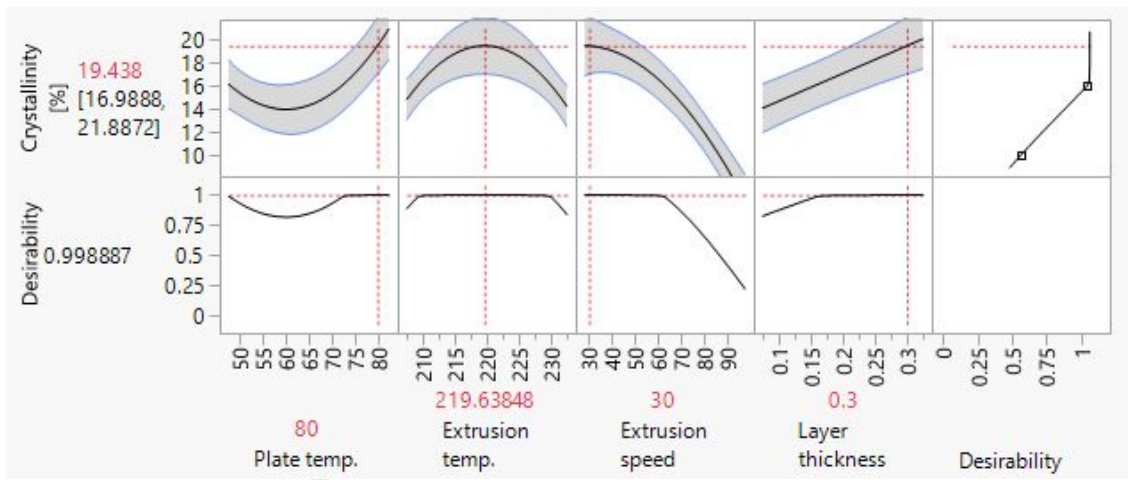
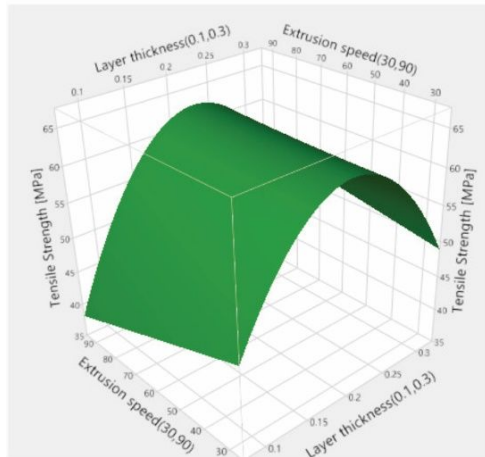
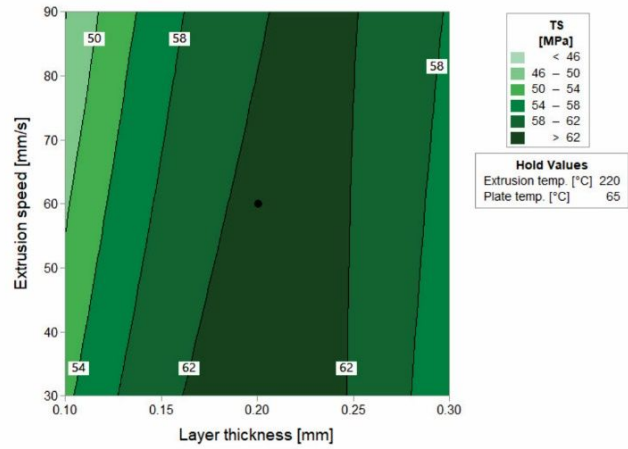


Fig. 3. Optimization plot for the Percent crystallinity experiment.

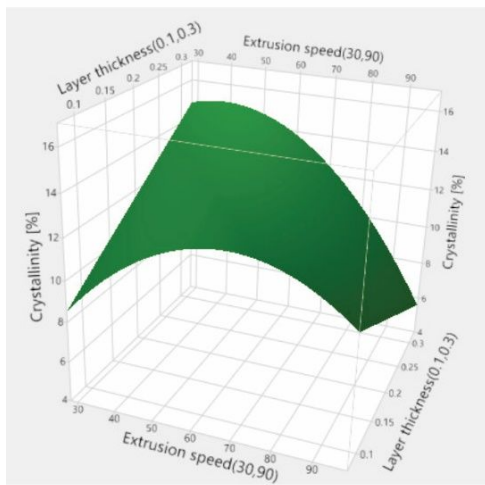
Rapid Prototyping Journal



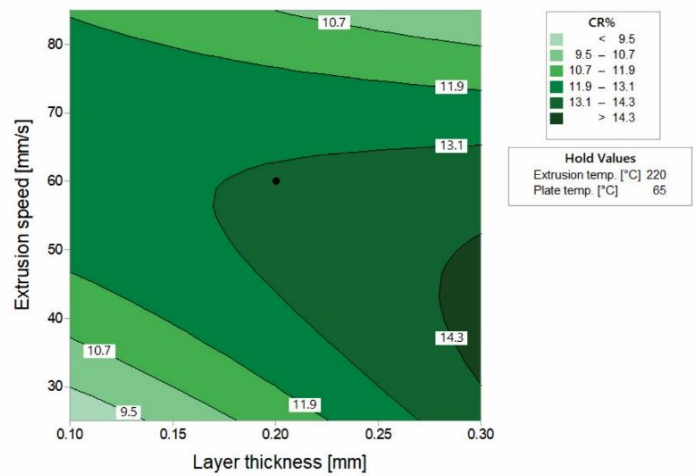
a)



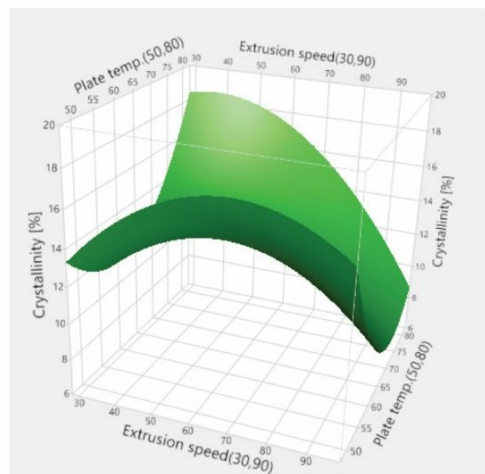
b)



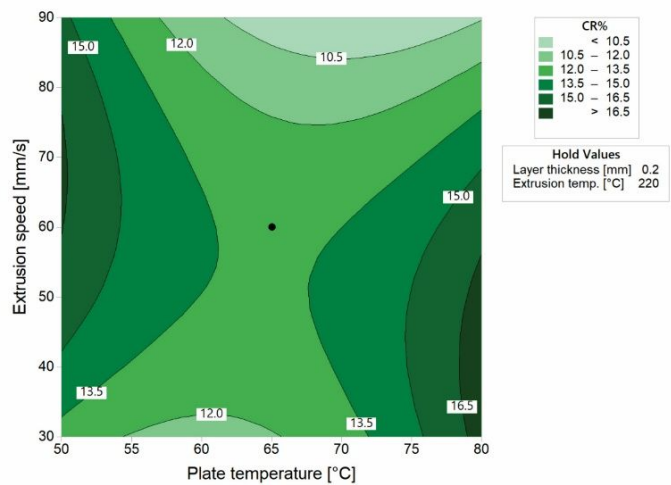
c)



d)



e)



f)

Fig. 4. Surface and contour plots for tensile strength analysis (a,b) and crystallinity analysis (c-f).

1
2
3
4
5
6
7
8
9
10
11
12
13
14
15
16
17
18
19
20
21
22
23
24
25
26
27
28
29
30
31
32
33
34
35
36
37
38
39
40
41
42
43
44
45
46
47
48
49
50
51
52
53
54
55
56
57
58
59
60

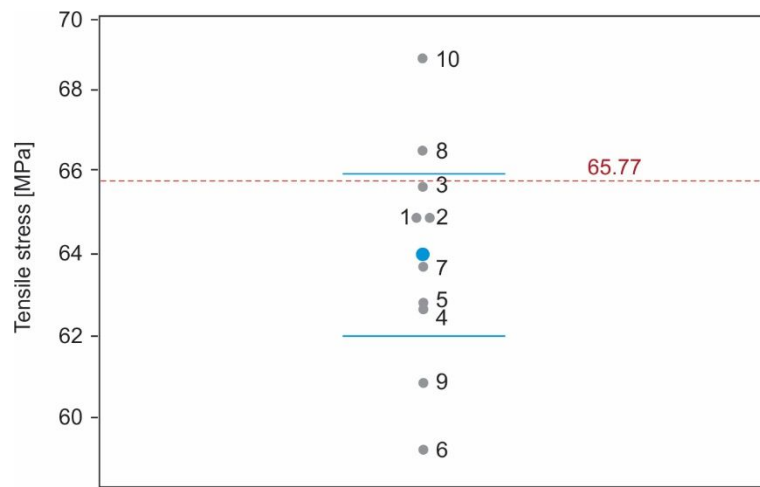


Fig. 5. A 95% Confidence Interval (blue horizontal lines) for the mean tensile strength constructed based on experimental verification data (Tab. 11), and the optimal tensile strength (red dotted line) obtained through optimization (Fig. 2).

Rapid Prototyping Journal

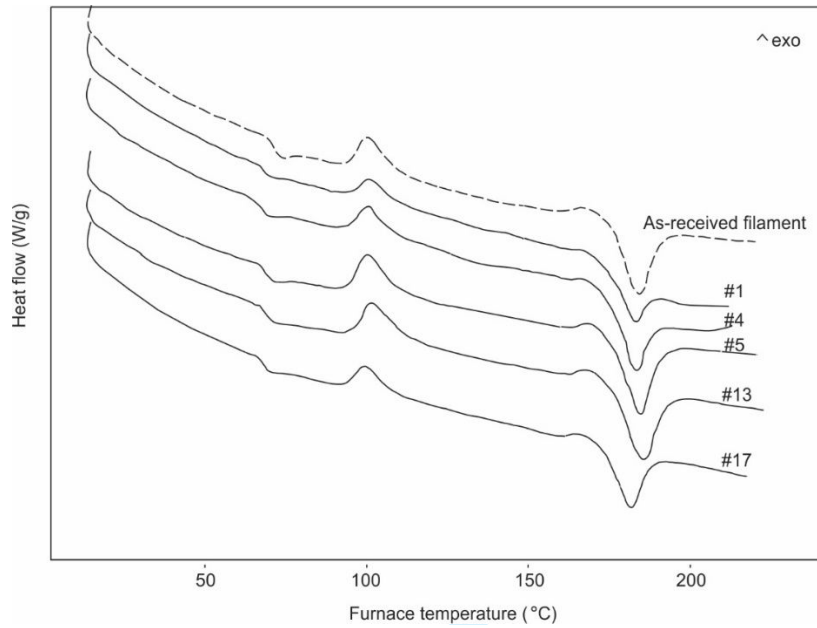


Fig. 6. DSC curves obtained for as-received filament and five samples from the design of experiment.

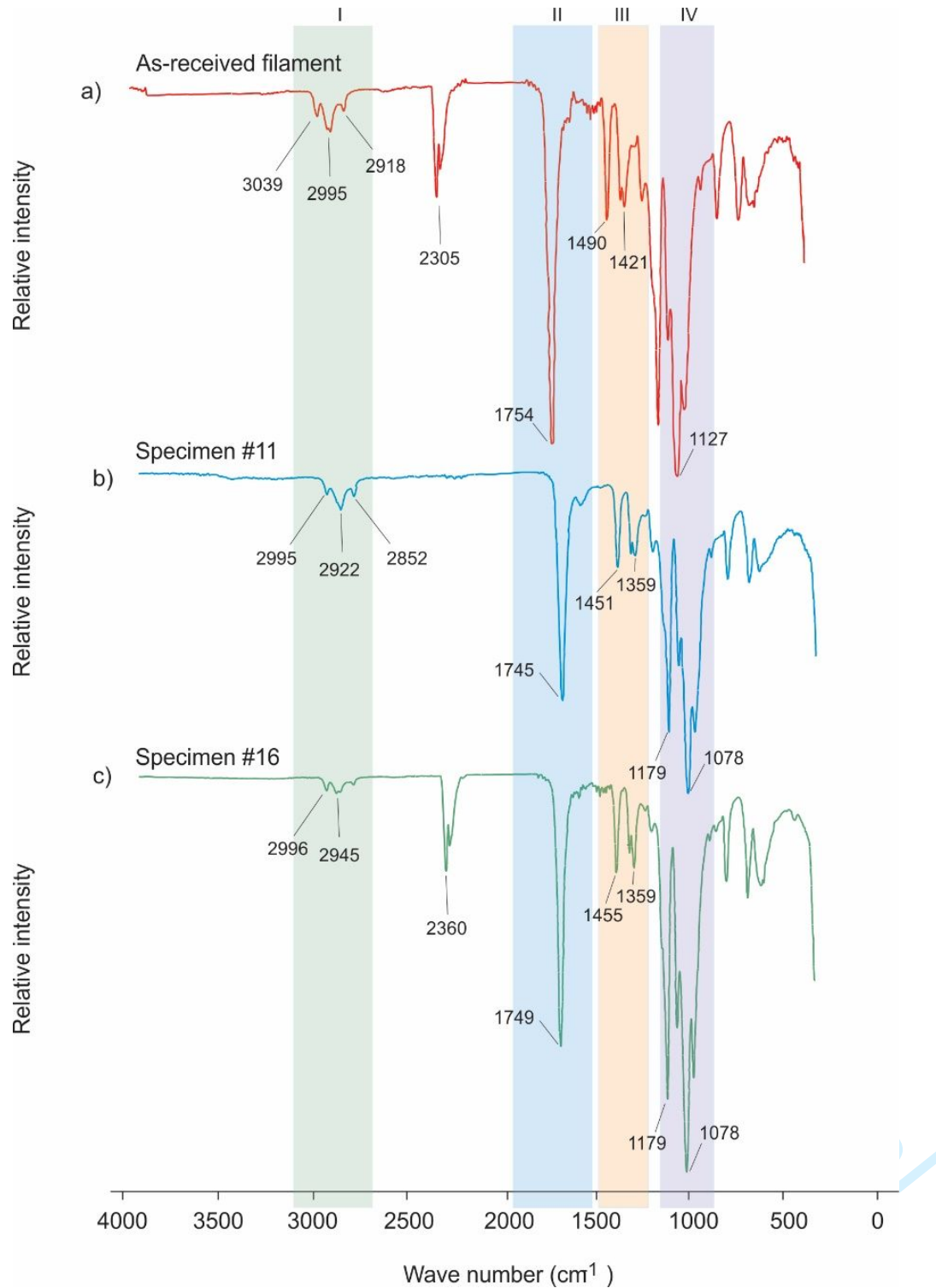


Fig. 7. FTIR diagrams for the as-received filament sample and two representative samples from the design of experiment.

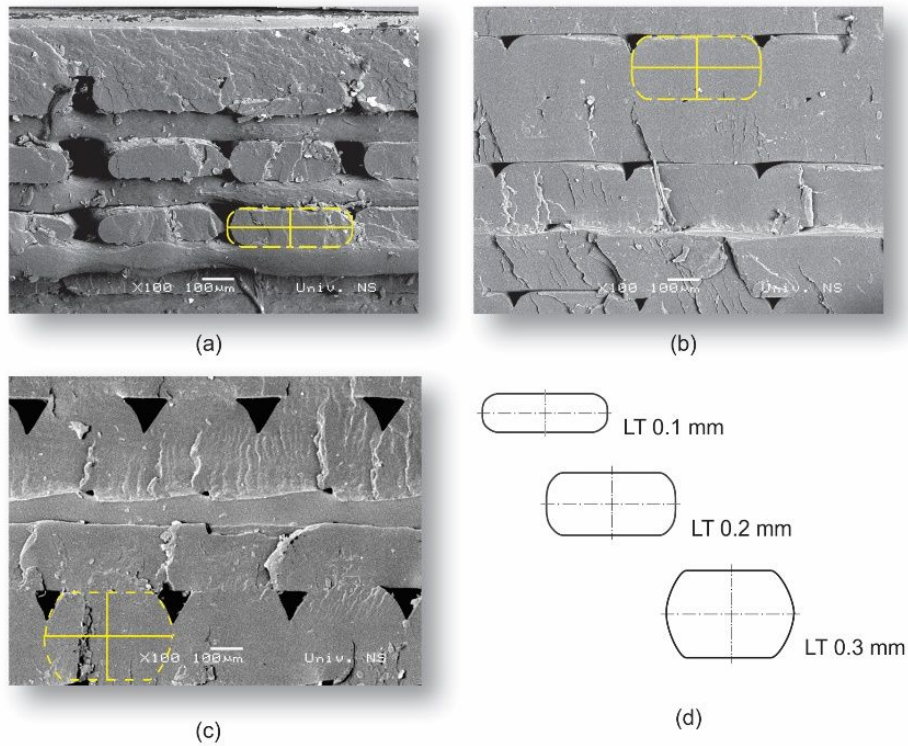


Fig. 8. Evolution of road cross-section geometry with the change of layer thickness: (a) $LT=0.1$ mm, (b) $LT=0.2$ mm, (c) $LT=0.3$ mm, (d) schematic comparison of the resulting geometries.

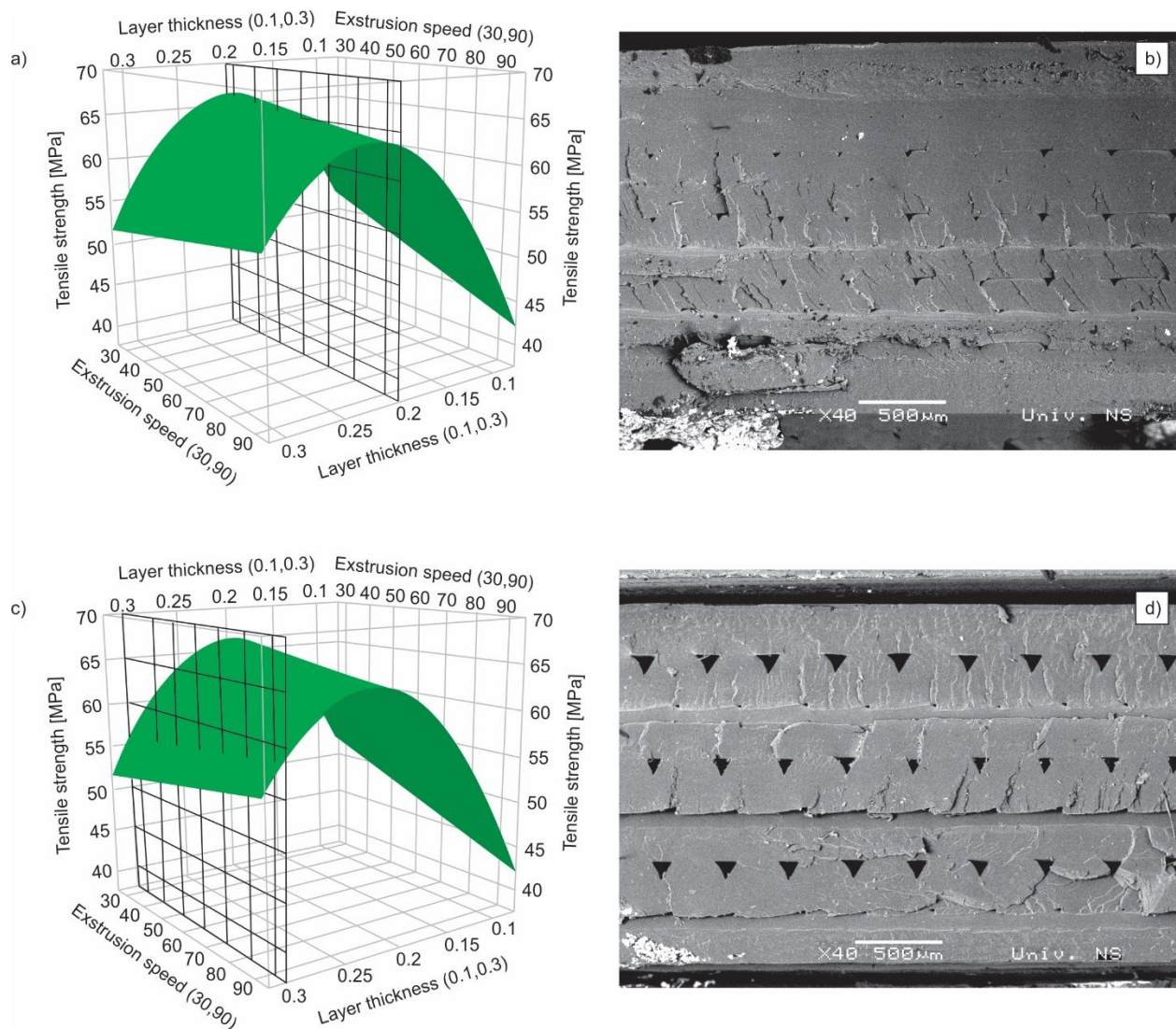


Fig. 9. Illustration of layer thickness impact on mesostructure - (a) surface plot obtained for optimal tensile stress settings, (b) cryo-fractured cross-sectional micrograph of a specimen printed with optimal settings, (c) surface plot obtained for the same settings as in (a), the only difference being layer thickness ($LT=0.3$ mm), which corresponds to the settings used for specimen #12 (Tab. 3), (d) cryo-fractured cross-sectional micrograph of specimen #12, showing significantly larger air gaps.

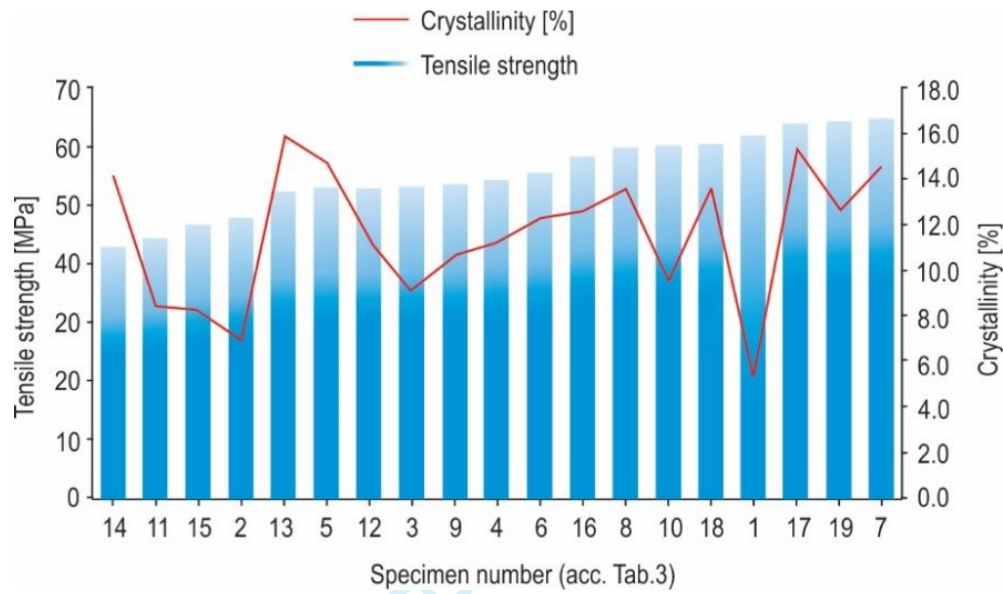


Fig. 10. Variation in percent crystallinity for the 19 specimens (Tab. 4) sorted by ascending tensile strength (Tab. 3).

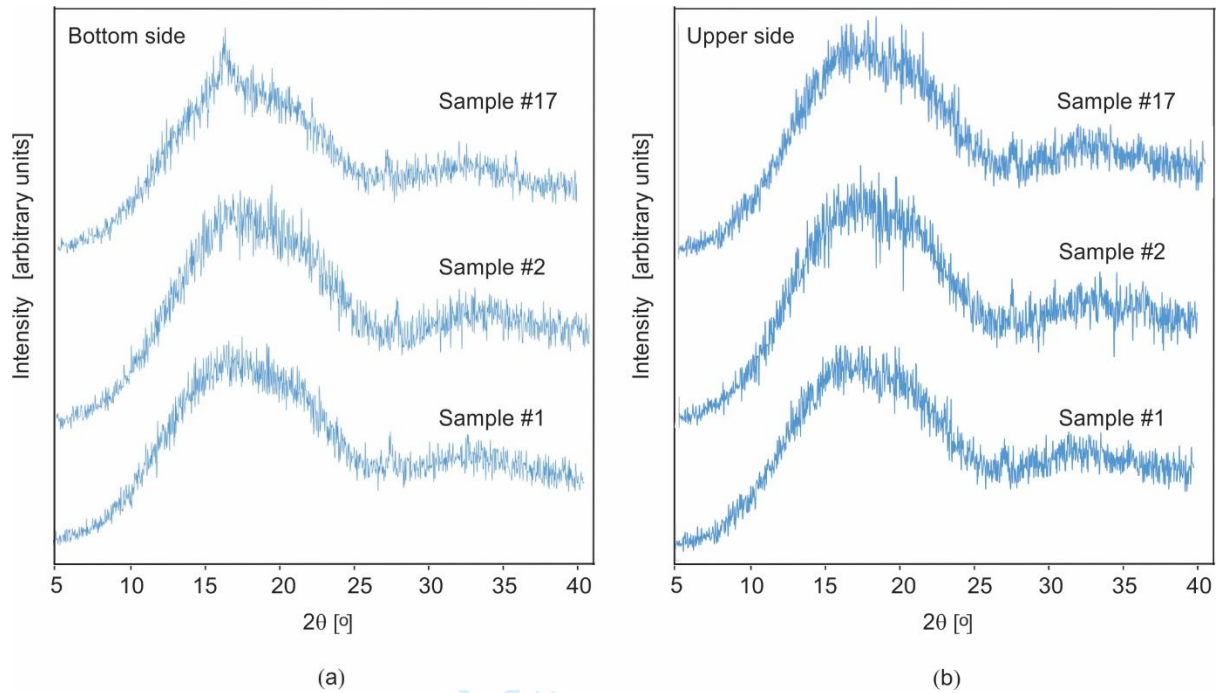


Fig. 11. XRD profiles of specimens #1, #2, and #17, for the bottom (a) and upper side (b).

Table 1. Factors, symbols, and level settings used in the experiment.

Factor	Symbol	Unit	Low level (-1)	Middle level (0)	High level (+1)
Layer thickness	LT	mm	0.1	0.2	0.3
Extrusion speed	ES	mm/s	30	60	90
Extrusion temperature	ET	°C	210	220	230
Build plate temperature	PT	°C	50	65	80

1
2
3
4
5
6
7
8
9
10
11
12
13
14
15
16
17
18
19
20
21
22
23
24
25
26
27
28
29
30
31
32
33
34
35
36
37
38
39
40
41
42
43
44
45
46
47
48
49
50
51
52
53
54
55
56
57
58
59
60

Table 2. Processing parameters kept at their fixed values during experiment.

Processing parameter	Value
No. of shells	2
No. of bottom layers	2
No. of top layers	2
Raster angle	0/90°
Infill	100%
Perimeter to raster air gap	0 mm
Fan speed (1 st layer off)	85-100%

Rapid Prototyping Journal

Table 3. DSD table with 19 experiments.

Exp.no.	LT [mm]	ES [mm/s]	ET [°C]	PT [°C]	Axial Force [N]	Tensile strength [MPa]
1.	0.3	90	230	65	504.6	63.08
2.	0.1	30	210	65	386.2	48.28
3.	0.3	90	220	80	426.9	53.36
4.	0.1	30	220	50	436.4	54.55
5.	0.3	60	210	80	423.3	52.91
6.	0.1	60	230	50	444.8	55.60
7.	0.2	30	210	80	518.9	64.86
8.	0.2	90	230	50	479.5	59.94
9.	0.1	30	230	80	428.0	53.50
10.	0.3	90	210	50	483.0	60.38
11.	0.1	90	210	80	356.0	44.50
12.	0.3	30	230	50	423.3	52.91
13.	0.3	30	230	80	420.9	52.61
14.	0.1	90	210	50	344.4	43.05
15.	0.1	90	230	80	375.4	46.93
16.	0.3	30	210	50	468.0	58.50
17.	0.2	60	220	65	513.0	64.13
18.	0.2	60	220	65	484.2	60.50
19.	0.2	60	220	65	514.0	64.25

Table 4. Results of crystallinity measurements for the 19 specimens, obtained by DSC analysis.

Exp. no.	Crystallization enthalpy ΔH_{cc} [J/g]	Re-crystallization enthalpy ΔH_r [J/g]	Melting enthalpy ΔH_m [J/g]	Crystallinity X_c [%]
1	18.357	6.407	29.697	5.3
2	19.478	6.041	31.945	6.9
3	19.363	5.333	33.123	9.1
4	19.782	6.027	36.118	11.1
5	21.384	4.151	39.163	14.7
6	18.554	6.086	36.047	12.3
7	21.160	4.061	38.658	14.4
8	18.433	4.559	35.575	13.5
9	20.712	5.641	36.203	10.6
10	18.066	5.343	32.196	9.4
11	17.971	6.520	32.313	8.4
12	19.781	4.644	35.049	11.4
13	19.798	3.910	38.540	15.9
14	15.942	4.645	33.720	14.1
15	19.44	5.649	32.829	8.3
16	18.506	4.599	34.804	12.6
17	18.034	4.846	37.116	15.3
18	16.453	4.685	33.714	13.5
19	17.342	5.030	34.189	12.7

Table 5. Parameter estimates for the Tensile strength experiment.

Term	Estimate	Std.error	t Ratio	Prob> t
Intercept	62.736	1.392034	45.07	<.0001
Layer thickness*Layer thickness	-9.93886	1.62167	-6.13	<.0001
Layer thickness (0.1,0.3)	3.31	0.831899	3.98	0.0022
Extrusion speed*Layer thickness	2.535857	0.9113	2.78	0.0178
Extrusion temp.*Layer thickness	-1.60986	0.9113	-1.77	0.105
Plate temp. (50,80)	-1.16143	0.831899	-1.4	0.1902
Extrusion speed (30,90)	-1.06929	0.831899	-1.29	0.2251
Extrusion temp. (210,230)	0.792143	0.831899	0.95	0.3614

1
2
3
4
5
6
7
8
9
10
11
12
13
14
15
16
17
18
19
20
21
22
23
24
25
26
27
28
29
30
31
32
33
34
35
36
37
38
39
40
41
42
43
44
45
46
47
48
49
50
51
52
53
54
55
56
57
58
59
60

Table 6. Summary of fit for the Tensile strength experiment.

Parameter	Value
RSquare	0.865461419
RSquare Adj	0.779845958
Root Mean Square Error	3.112682228
Mean of Response	55.41263158
Observations (or Sum Wgts)	19

Rapid Prototyping Journal

Table 7. ANOVA table for the Tensile strength experiment.

Source	DF	Sum of Squares	Mean Square	F Ratio	Prob > F
Model	7	685.5879	97.9411	10.1087	0.0005
Error	11	106.5767	9.6888		
C. Total	18	792.1646			

Rapid Prototyping Journal

Table 8. Parameter estimates for the Percent crystallinity experiment.

Term	Estimate	Std Error	t Ratio	Prob> t
Intercept	13.22399	0.540378	24.47	<.0001*
Plate temp.*Extrusion speed	-2.262184	0.312616	-7.24	<.0001*
Extrusion speed*Layer thickness	-1.912027	0.321437	-5.95	0.0002*
Plate temp.*Plate temp.	3.1011048	0.617415	5.02	0.0007*
Extrusion temp.*Extrusion temp.	-3.16108	0.680898	-4.64	0.0012*
Extrusion speed (30, 90)	-1.057143	0.25809	-4.10	0.0027*
Extrusion speed*Extrusion speed	-2.386869	0.625232	-3.82	0.0041*
Layer thickness (0.1, 0.3)	0.4785714	0.25809	1.85	0.0967
Extrusion temp. (210, 230)	-0.228571	0.25809	-0.89	0.3989
Plate temp. (50, 80)	-0.214286	0.25809	-0.83	0.4279

Table 9. Summary of fit for the Percent crystallinity experiment.

Parameter	Value
RSquare	0.94338
RSquare Adj	0.88676
Root Mean Square Error	0.965683
Mean of Response	11.42105
Observations (or Sum Wgts)	19

1
2
3
4
5
6
7
8
9
10
11
12
13
14
15
16
17
18
19
20
21
22
23
24
25
26
27
28
29
30
31
32
33
34
35
36
37
38
39
40
41
42
43
44
45
46
47
48
49
50
51
52
53
54
55
56
57
58
59
60

Table 10. ANOVA table for the Percent crystallinity experiment.

Source	DF	Sum of Squares	Mean Square	F Ratio
Model	9	139.83869	15.5376	16.6616
Error	9	8.39289	0.9325	Prob > F
C. Total	18	148.23158		0.0001*

Rapid Prototyping Journal

Table 11. Ten verification measurements of tensile stress, obtained for the specimens fabricated with optimal settings shown in Fig. 2.

Force [N]	518.9	518.9	524.9	501.1	502.2	473.5	509.3	532.1	486.6	550.1
T.Stress [MPa]	64.86	64.86	65.61	62.62	62.77	59.19	63.66	66.51	60.825	68.76

Table 12. Five verification measurements of percent crystallinity, obtained for the specimens fabricated with optimal settings shown in Fig. 3.

Exp. no.	Crystallization enthalpy ΔH_{cc} [J/g]	Re-crystallization enthalpy ΔH_r [J/g]	Melting enthalpy ΔH_m [J/g]	Crystallinity X_c [%]
1	19.119	4.162	34.913	12.5
2	18.121	3.084	36.702	16.7
3	21.563	3.989	41.419	17.1
4	19.801	4.041	39.224	16.5
5	20.098	3.433	41.780	19.6